Orbital-Angular-Momentum Mode Selection by Rotationally Symmetric Superposition of Chiral States with Application to Electron Vortex Beams

Yuanjie Yang,[1,2] G. Thirunavukkarasu,[1] M. Babiker,[1] and Jun Yuan[1,*]
[1]Department of Physics, University of York, Heslington, York YO10 5DD, United Kingdom
[2]School of Astronautics & Aeronautics, University of Electronic Science and Technology of China, Chengdu 611731, China
(Received 6 January 2017; published 31 August 2017)

A general orbital-angular-momentum (OAM) mode selection principle is put forward involving the rotationally symmetric superposition of chiral states. This principle is not only capable of explaining the operation of vortex generating elements such as spiral zone plate holograms, but more importantly, it enables the systematic and flexible generation of structured OAM waves in general. This is demonstrated both experimentally and theoretically in the context of electron vortex beams using rotationally symmetric binary amplitude chiral sieve masks.

DOI: 10.1103/PhysRevLett.119.094802

Vortices are common to all wave phenomena [1], including tornadoes at the large scale and superfluid helium at the small scale. Optical vortex beams have been intensively studied due to their quantized orbital-angular-momentum (OAM) character [2]. This was followed recently by the study of electron vortex beams [3–5] and there are early studies of neutron [6] and atom vortex beams [7]. Vortex beams are characterized by a phase singularity described by an $\exp(i\ell\theta)$ azimuthal phase factor, where θ is the azimuthal angle and ℓ stands for the winding number and is also called the topological charge. Vortex beams are of special interest because of their quantized OAM of $\ell\hbar$ per particle [1] and have led to various applications in the contexts of super-resolution microscopy [8], nanomanipulation [9], astronomy [10], and crystallography [11]. In contrast to the intrinsic (spin) angular momentum, OAM can be very large and, as such, vortex beams can lead to new physics [12,13] and have potential in multiplex free-space communication [14] and quantum information [15].

The establishment of a toolbox for flexible vortex beam generation is the key to the development of science and technology involving vortex beams. If the vortex beam wave functions are known exactly, they can be generated by direct phase manipulation (or wave front shaping) [16] using, for example, spiral phase plates [3,6,17], spin-to-orbital angular momentum convertors [18], and by phase encoding techniques through diffraction involving computer-generated holograms (CGHs) [19], including fork grating [4,5] and spiral zone plates [20–22]. Other techniques require case-by-case analysis to identify the nature of the vortex beams produced, as in the case involving the Aharonov-Bohm effect experienced by a charged particle in a suitable magnetic field [23,24]. More recent methods make use of photon sieves [25–27] and Vogel spiral arrays [28,29] as diffractive elements for vortex beam generation.

Here we put forward a general principle for vortex beam generation in rotationally symmetric systems. We examine the role of rotational symmetry, not only for the purpose of generating a specific vortex wave function, but also for the essential symmetry elements that must be possessed by any vortex-related state by virtue of its characteristic azimuthal phase factor $\exp(i\ell\theta)$. The principle would enable us to understand, in a novel deconstructive manner, the generation of individual pure vortex beams using a diverse range of rotationally symmetric optical elements, such as spiral diffractive holograms (spiral zone plates) [20–22], two-dimensional chiral cam-shaped objects [30], and plasmonic vortex lens [31]. Furthermore, the study of rotational symmetry in the vortex context would provide a useful guide for exploring a broader range of vortex-related beams, including those with complex vortex characters, such as vortex modes that consist of a mixture of concentric vortex states each with a different OAM content.

The principle in question emerges from the following analysis. Consider the scenario in which m identically monochromatic wavelets are equally spaced in the azimuthal angular domain. Let $u(\rho, z, \theta + 2\pi s/m)$ be the complex amplitude of the sth wavelet in cylindrical polar coordinates. Then the total field due to the rotationally symmetric superposition of m such wavelets is the sum

$$\psi(\rho, z, \theta) = \sum_{s=0}^{m-1} u\left(\rho, z, \theta + \frac{2\pi s}{m}\right). \tag{1}$$

The individual amplitude function $u(\rho, z, \theta)$ can be expressed in terms of any complete orthonormal basis set such as the set of Laguerre-Gaussian (LG) modes [15]. A useful alternative would be the complete set of the Fourier transforms of the truncated Bessel functions [32]. We consider here the use of the LG set and write

$$u(\rho, z, \theta) \propto \sum_{p=0}^{\infty} \sum_{\ell=-\infty}^{\infty} c_{p,\ell}\varphi_{p,\ell}(\rho, z, \theta), \tag{2}$$

 © 2017 American Physical Society

where $\varphi_{p,\ell}(\rho,z,\theta)$ denotes a LG mode of radial and azimuthal indices (p,ℓ) and the expansion coefficients $c_{p,\ell}=\iint u(\rho,z,\theta)\varphi^{*}_{p,\ell}(\rho,z,\theta)\rho d\rho d\theta$ are the overlap integrals. Substituting Eq. (2) into Eq. (1) we have

$$\psi(\rho,z,\theta)=\sum_{s=0}^{m-1}\sum_{p=0}^{\infty}\sum_{\ell=-\infty}^{\infty}c_{p,\ell}\varphi_{p,\ell}\left(\rho,z,\theta+\frac{2\pi s}{m}\right). \quad (3)$$

The LG modes have the form $\varphi_{p,\ell}(\rho,z,\theta)=A_{p,\ell}(\rho,z)\exp(i\ell\theta)$ where the $A_{p,\ell}(\rho,z)$'s are the mode amplitude functions. Once this form of $\varphi_{p,\ell}(\rho,z,\theta)$ is inserted in Eq. (3), it becomes clear that the finite series summation over s is just a geometrical series summation that yields

$$S=\sum_{s=0}^{m-1}\exp\left(i\ell\frac{2\pi s}{m}\right)=\frac{1-\exp(i\ell\frac{2\pi m}{m})}{1-\exp(i\ell\frac{2\pi}{m})}=\begin{cases}m, & \ell=Mm\\ 0, & \ell\neq Mm\end{cases}, \quad (4)$$

where M is an integer, namely, $M=0,\pm1,\pm2,\ldots$. As a result, Eq. (3) gives

$$\psi(\rho,\theta,z)=\begin{cases}m\sum_{\ell}\sum_{p=0}^{\infty}c_{p,\ell}A_{p,\ell}(\rho,z)\exp(i\ell\theta), & \ell=Mm\\ 0, & \ell\neq Mm\end{cases} \quad (5).$$

Recall that m is the number of angularly equally spaced wavelets and M is an integer. Equation (5) embodies what we call the principle of rotationally symmetric superposition of chiral states and has two interesting consequences.

(i) If the initial wavelets are pure vortex beam states with well-defined OAM, then Eq. (5) is reduced to

$$\psi(\rho,\theta,z)=\begin{cases}mu(\rho,z,\theta), & \ell=Mm\\ 0, & \ell\neq Mm\end{cases}, \quad (6)$$

which means that the superposition of LG modes is nonvanishing only when the topological charge ℓ is a multiple of m, the number of wavelets.

(ii) If the initial wavelets are not vortex states with pure OAM modes, then Eq. (5) shows that the superposition of m such wavelets can produce vortex beams with OAM modes $\ell=0,\pm m,\pm 2m,\ldots$; this is "OAM combing" by imposing rotational symmetry. If a specific single OAM mode is required out of the multiple OAM harmonics allowed by the rotational symmetry of the system, two further steps would be needed to achieve that goal: (1) the inclusion of chiral symmetry to break the mirror symmetry; and (2) the selection of a particular OAM mode by "spatial filtering." This is based on the fact that the size of an OAM mode scales with its topological charge [33]. Furthermore, the superposition principle in question is particularly suitable in applications involving the generation of high order OAM vortex beams.

As a first illustration of these OAM combing and filtering processes we consider how to generate a pure vortex beam with a specific topological charge. In this example the wavelets are due to diffracted beams from plane waves passing through a rotationally symmetric arrangement of pinholes, as shown in Fig. 1. The result of the superposition is observed in a plane distance z away. The diffracted beam from each pinhole contains a geometrical phase factor that can be manipulated by adjusting the geometry and positions of the pinholes, as we now explain. Figure 1(a) shows the simplest case of a fivefold rotationally symmetric achiral mask consisting of only five pinholes. When the mask is illuminated by a plane wave, it leads to the intensity and phase patterns at the observation z plane as shown in Figs. 1(b) and 1(c), respectively.

The theoretical relative power of the individual modes emerging on illumination is obtainable by the decomposition of the complex field in terms of the LG basis set [15], followed by subsequent summation over all the p modes with the same topological charge ℓ. The power spectrum corresponding to the mask in Fig. 1(a) is displayed in

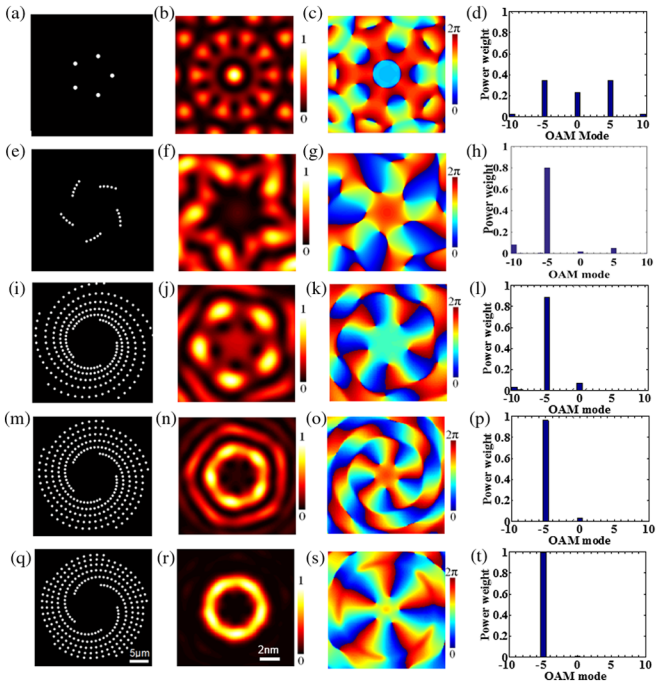

FIG. 1. Management of the OAM modes using rotationally symmetric masks constructed from different rotationally symmetric motifs: (a) the five-pinhole mask, (b) the simulated intensity pattern and (c) phase pattern at defocus $\Delta f=-33.6$ μm, and (d) the corresponding power spectra in the OAM mode ℓ. (e)–(h) are based on five short pinhole curves (motifs). (i)–(l) are based on logarithmic spirals. (m)–(p) are based on Archimedean spirals. (q)–(t) are based on the Fermat spirals. Here, the expansion area of the complex fields that were decomposed into the LG basis set was 10×10 nm.

Fig. 1(d), which shows that the five-pinhole mask converts a plane wave into a set of OAM modes with $\ell = 0, \pm 5, \pm 10$ (within the ± 10 range of the plot shown), which is consistent with the result in Eq. (5). The symmetric distribution of the power spectrum is indicative of the mirror symmetry of the pinhole arrangement.

In order to generate vortex beams with chiral phase structures, we have to deal with a chiral rotationally symmetric pinhole array mask. The first example of such a mask is shown in Fig. 1(e) consisting of five short pinhole "motifs" each with several pinholes arranged as shown. For an effective vortex beam production, individual motifs in the designed mask would typically consist of many pinholes distributed along a number of spirals. Spiral pinhole motifs are particularly attractive as the corresponding masks have a clear handedness, giving rise to an azimuthal phase ramp in the diffracted waves near the beam axis due to angular dependent distance from the pinholes to the axis, i.e., $c_{p,\ell} \neq c_{p,-\ell}$ in Eq. (5). The corresponding OAM mode spectrum shown in Fig. 1(h) is seen to be dominated by the $\ell = -5$ mode. The power weights of the other modes are very low, as desired. This OAM selection ability is a major feature of the principle we have introduced above.

To explore this OAM-dependent on-axis focusing effect of the chiral multiple-pin-hole mask, we have considered pinhole masks in which the basic unit motifs are in the form of well-known spirals. The last three rows in Fig. 1 show the cases of spiral-pinhole masks involving Logarithmic [$\rho \propto a \exp(b\theta)$], Archimedean [$\rho \propto (a + b\theta)$], and Fermat spiral motifs. In the case of the Fermat spiral, N pinholes are distributed along each spiral motif according to $\alpha_n = 2\pi n/N$ and $r_n = (r_0^2 + \ell z \lambda \alpha_n/\pi)^{1/2}$, where λ is the wavelength of the incident wave, z is the observation plane, and r_0 is the coordinate of the first pinhole from the center [34]. The results of the OAM mode analysis for this case are shown in Figs. 1(l), 1(p), and 1(t). These results indicate that the purity of the OAM of the vortex modes generated near the beam axis can be progressively tuned by using masks based on different kinds of spirals.

The rotationally symmetric arrangement of ℓ Fermat spiral motifs reinforces the strength of the allowed OAM modes generated by individual motifs, while filtering out the neighboring symmetry-incompatible OAM modes, resulting in the purist on-axis OAM mode, as shown by the OAM spectrum in Fig. 1(t) [also see Fig. S1 in Supplemental Material (SI) for more details [35]]. The resulting spiral multipinhole mask shown in Fig. 1(q) may be considered as a simplified version of the spiral diffraction grating mask designed to produce a pure vortex beam of winding number ℓ at the observation plane. Unlike the spiral CGH mask, the multipinhole masks are easy to manufacture and are mechanically more robust since our deconstructive analysis allows us to retain the essential features required for the pure vortex beam generation while achieving similar vortex beam conversion efficiency (see Fig. S2 in SI for more details [35]).

However, the true power of our "deconstructed approach" lies in the considerable degree of freedom afforded by the systematic and rational design of more realistic and complex vortex beam approximates that, to date, are difficult to foresee and achieve, either by the traditional CGH approach or by those based on other *ad hoc* bases [28,29].

To illustrate the new insight gained from our analysis, we next consider the compact pinhole mask shown in Fig. 2(a). This kind of mask design is shown to be suitable for the production of vortex beams with more complicated spatial structures. The mask in Fig. 2(a) is designed to have 11 Fermat spirals (red), each of which is the same as that given in Fig. 1(q). Because of the degeneracy, two additional spirals with repetition of 44 (yellow spirals) and 55 (green spirals) can be identified. Moreover, the handedness of the yellow spirals is opposite to those of the red and green spirals. According to the above analysis, we expect each of such regular spiral arrangements to support an OAM mode. Unlike the vortex beams generated by the spiral CGH masks where different OAM modes are focused at different on-axis positions while other OAM modes exist only as a complex mixture in the background, our mask generates a beam with three bright rings corresponding to the three sets

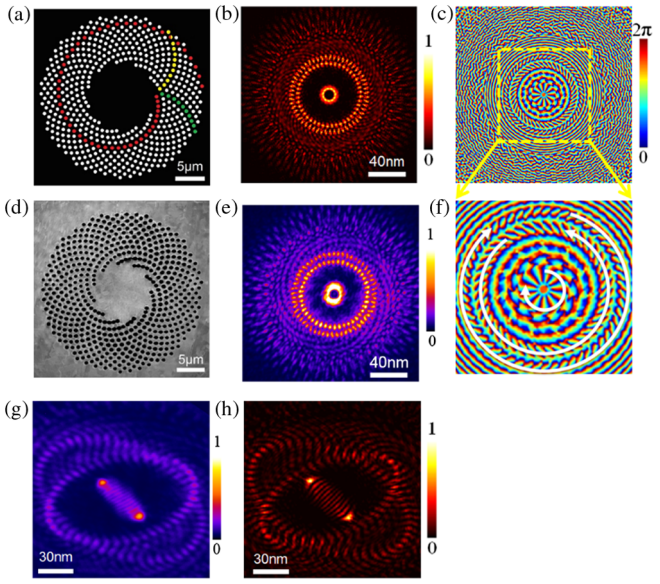

FIG. 2. Generation of concentric electron vortex beams and the measurement of their topological charges. (a) Simulation of a structured electron sieve. [(b) and (c)] The corresponding simulations of the intensity (b) and phase (c) at defocus $\Delta f = -74.6$ μm. (d) The scanning electron microscope image of the electron sieve. (e) The experimental results of the intensity patterns. (f) A zoomed-in view of the center part of (c). The white curves in (f) indicate increasing direction of phase. [(g) and (h)] The experimental results (g) and the corresponding simulation (h) of the intensity pattern after astigmatic transformation.

of spiral patterns in the mask [Fig. 2(b)], with the outer two rings having 44 and 55 bright dots, respectively. The simulated phase map of the diffracted beams shown in Figs. 2(c) and 2(f) suggests that the total phase change for each over a complete revolution is by $-11 \times 2\pi$ around the center, by $44 \times 2\pi$ and $-55 \times 2\pi$ in the corresponding regions of two necklacelike beams in the clockwise direction. This shows that the "sievelike" mask has generated a compound vortex beam containing simultaneously three copropagating vortex beams with topological charges $\ell = -11$, 44, and -55, respectively. As we show in Fig. S3 in the SI [35], the secondary high OAM modes can be controlled by changing the number of holes in each of the Fermat spiral motifs.

Note that our analysis is general and is therefore applicable to any vortex states that can be described by a scalar wave equation, such as optical vortex beams, electron vortex beams, and other matter vortex beams.

We now provide a description of the experimental work we have carried out to test the above theoretical predictions applicable in the context of electron vortex beams. The physical mask presented in Fig. 2(d) was created from a 1 μm thick Pt foil and the radius of each pinhole $a = 300$ nm. We illuminated the mask with a relatively coherent electron beam in a JEOL 2200FS TEM operating at 200 kV, which corresponds to an electron de Broglie wavelength of $\lambda = 2.5$ pm. The mask was inserted in the condenser aperture of the electron microscope. Instead of observing the pattern directly, the condenser lens was turned on and the observation is conducted at the corresponding defocus distance from the focal plane of the condenser lens, which has a focal length of about 15 mm. Figure 2(e) displays the experimental intensity pattern bearing three rings, in good agreement with the simulated intensity pattern [Fig. 2(b)]. It is well known that the vortex modes can be astigmatically transformed into Hermite-Gausslike modes, with the number of dark stripes indicating the value of the OAM carried by the vortex [32,36]. The experimental intensity pattern [Fig. 2(g)] and the corresponding simulation result [Fig. 2(h)] of the vortex beam after the astigmatic transformation show that indeed there are 11 dark stripes in the center, with respect to the tilt direction, confirming that the inner ring of the emerging beam is a vortex beam with topological charge $\ell = -11$. Furthermore, both Fig. 2(g) and Fig. 2(h) also exhibit two ellipses tilted in different directions, consistent with the fact that the topological charges of the two outer rings of the intensity pattern [Figs. 2(b) and 2(e)] do indeed have opposite signs [36].

We can further explore the characteristics of the electron vortex state consisting of three copropagating OAM modes by following the evolution of the intensity distribution near the focal plane ($P4$ in Fig. 3) of the condenser lens. The experimental observation displayed together with the simulated normalized intensity distribution in the y-z plane in Fig. 3 constitutes a clear agreement, including the

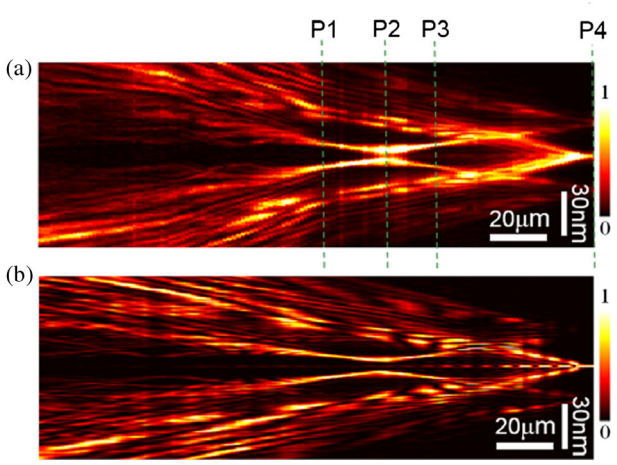

FIG. 3. The propagation of vortex beams generated by electron sieves. (a) Experimental results of the intensity pattern in the y-z plane. (b) The corresponding result of simulation. The experimental result in (a) was reconstructed from 140 slices of the x-y plane intensity pattern recorded in the experiment. $P1$–$P4$ represent four transverse planes perpendicular to the propagation axis. $P2$ corresponds to the intensity patterns shown in Fig. 2(e), and $P4$ denotes the focal plane of the condenser lens.

confirmation that the Fermat spirals have led to an OAM mode of topological charge of magnitude 11, which has its beam waist at the observation plane $\Delta f = -74.6$ μm ($P2$ in Fig. 3). The two other spirals in the sieve mask are non-Fermat-like and hence have no clear beam waist at the plane $P2$. The different focusing behaviors of the three vortex rings also mean they have different Gouy phase change near the observation plane. This is consistent with the different stages of the astigmatic transformation of the three OAM rings seen in Figs. 2(g) and 2(h). The supplemental movie indicated in SI [35] shows that these outer two necklacelike rings have opposite senses of rotation and each maintains its fixed number of pearls when they propagate from plane $P1$ to plane $P3$, demonstrating the correct identification of the helicities of the vortex modes.

We reiterate that our general design approach and the results we have obtained with electron sieve masks are also applicable to other matter waves as well as optical vortex beams. A specific advantage of the methods we have described is that it can produce complicated structured beams, such as concentric electron vortices and optical vortices, which carry different OAMs with different radii. These vortex beams with superposition of OAM states are of importance in classical physics and quantum science. For example, they may be used in the manipulation of fluid-borne particles and also as a nano-optomechanical Couette shear cell [37] as well as in multiplex broadband communication.

In conclusion, we have put forward and demonstrated the utility of a fundamental superposition and selection principle of OAM modes. This constitutes a new approach in

the design of convertors for structured beam generation from plane waves, providing a versatile and robust alternative to the conventional CGH approach. Our analysis provides a new understanding of the essential components of the OAM conversion process by rotationally symmetric wave-optical structures. It is applicable to the generation and analysis of OAM distributions of all scalar waves in axially symmetric systems.

This work is supported by the Engineering and Physical Sciences Research Council Grants No. EP/G070474/1 and No. EP/G070326/1. We also acknowledge support from the European Cooperation in Science and Technology, Grant No. MP0903. Y. J. Y. acknowledges the support by the National Natural Science Foundation of China under Grants No. 61205122 and No. 11474048.

*Corresponding author.
jun.yuan@york.ac.uk

[1] J. F. Nye and M. V. Berry, Proc. R. Soc. A **336**, 165 (1974).
[2] L. Allen, M. W. Beijersbergen, R. J. C. Spreeuw, and J. P. Woerdman, Phys. Rev. A **45**, 8185 (1992).
[3] M. Uchida and A. Tonomura, Nature (London) **464**, 737 (2010).
[4] J. Verbeeck, H. Tian, and P. Schattschneider, Nature (London) **467**, 301 (2010).
[5] B. J. McMorran, A. Agrawal, I. M. Anderson, A. A. Herzing, H. J. Lezec, J. J. McClelland, and J. Unguris, Science **331**, 192 (2011).
[6] C. W. Clark, R. Barankov, M. G. Huber, M. Arif, D. G. Cory, and D. A. Pushin, Nature (London) **525**, 504 (2015).
[7] V. E. Lembessis, D. Ellinas, M. Babiker, and O. Al-Dossary, Phys. Rev. A **89**, 053616 (2014).
[8] S. W. Hell and J. Wichmann, Opt. Lett. **19**, 780 (1994).
[9] K. Dholakia and T. Cizmar, Nat. Photonics **5**, 335 (2011).
[10] G. A. Swartzlander, Jr., E. L. Ford, R. S. Abdul-Malik, L. M. Close, M. A. Peters, D. M. Palacios, and D. W. Wilson Opt. Express **16**, 10200 (2008).
[11] R. Juchtmans, A. Béché, A. Abakumov, M. Batuk, and J. Verbeeck, Phys. Rev. B **91**, 094112 (2015).
[12] I. P. Ivanov and D. V. Karlovets, Phys. Rev. Lett. **110**, 264801 (2013).
[13] J. Harris, V. Grillo, E. Mafakheri, G. C. Gazzadi, S. Frabboni, R. W. Boyd, and E. Karimi, Nat. Phys. **11**, 629 (2015).
[14] J. Wang, J. Yang, I. Fazal, N. Ahmed, Y. Yan, H. Huang, Y. Ren, Y. Yue, S. Dolinar, M. Tur, and A. Willner, Nat. Photonics **6**, 488 (2012).
[15] G. Molina-Terriza, J. P. Torres, and L. Torner, Phys. Rev. Lett. **88**, 013601 (2001).
[16] *The Angular Momentum of Light* edited by D. L. Andrews and M. Babiker (Cambridge University Press, Cambridge, 2012).
[17] M. W. Beijersbergen, R. P. C. Coerwinkel, and M. Kristensen, Opt. Lett. **112**, 321 (1994).
[18] L. Marrucci, C. Manzo, and D. Paparo, Phys. Rev. Lett. **96**, 163905 (2006).
[19] V. Grillo, G. C. Gazzadi, E. Mafakheri, S. Frabboni, E. Karimi, and R. W. Boyd, Phys. Rev. Lett. **114**, 034801 (2015).
[20] N. R. Heckenberg, R. McDuff, C. P. Smith, and G. White, Opt. Lett. **17**, 221 (1992).
[21] J. Verbeeck, H. Tian, and A. Béché, Ultramicroscopy **113**, 83 (2012).
[22] K. Saitoh, Y. Hasegawa, N. Tanaka, and M. Uchida, J. Electron Microsc. **61**, 171 (2012).
[23] L. Clark, A. Béché, G. Guzzinati, A. Lubk, M. Mazilu, R. Van Boxem, and J. Verbeeck, Phys. Rev. Lett. **111**, 064801 (2013).
[24] A. Béché, R. Van Boxem, G. Van Tendeloo, and J. Verbeeck, Nat. Phys. **10**, 26 (2013).
[25] C. Xie, X. Zhu, L. Shi, and M. Liu, Opt. Lett. **35**, 1765 (2010).
[26] R. Liu, F. Li, M. J. Padgett, and D. B. Phillips, Optica **2**, 1028 (2015).
[27] K. Huang, H. Liu, F. J. Garcia-Vidal, M. Hong, B. Luk'yanchuk, J. Teng, and C. Qiu, Nat. Commun. **6**, 7059 (2015).
[28] N. Lawrence, J. Trevino, and L. Dal Negro, Opt. Lett. **37**, 5076 (2012).
[29] L. Dal Negro, N. Lawrence, and J. Trevino, Opt. Express **20**, 18209 (2012).
[30] O. Emile, M. Le Meur, and J. Emile, Phys. Rev. A **89**, 013846 (2014).
[31] H. Kim, J. Park, S. Cho, S. Lee, M. Kang, and B. Lee, Nano Lett. **10**, 529 (2010).
[32] G. Thirunavukkarasu, M. Mousley, M. Babiker, and J. Yuan, Phil. Trans. R. Soc. A **375**, 20150438 (2017).
[33] J. E. Curtis and D. G. Grier, Phys. Rev. Lett. **90**, 133901 (2003).
[34] Z. Li, M. Zhang, G. Liang, X. Li, X. Chen, and C. Cheng, Opt. Express **21**, 15755 (2013).
[35] See Supplemental Material at http://link.aps.org/supplemental/10.1103/PhysRevLett.119.094802, which includes three figures and a movie showing the propagation of the electron vortex beams generated by electron sieves.
[36] R. Shiloh, Y. Tsur, R. Remez, Y. Lereah, B. A. Malomed, V. Shvedov, C. Hnatovsky, W. Krolikowski, and A. Arie, Phys. Rev. Lett. **114**, 096102 (2015).
[37] K. Ladavac and D. G. Grier, Europhys. Lett. **70**, 548 (2005).